OXFORD

Cerebral Cortex, 2023, **33**, 10272–10285
https://doi.org/10.1093/cercor/bhad281
Advance access publication date 11 August 2023
Original Article

DOT1L deletion impairs the development of cortical parvalbumin-expressing interneurons

Arquimedes Cheffer[1,†], Marta Garcia-Miralles[1,†], Esther Maier[1,†], Ipek Akol[1,2], Henriette Franz[1], Vandana Shree Vedartham Srinivasan[1], Tanja Vogel[1,3,*]

[1]Department of Molecular Embryology, Medical Faculty, Institute of Anatomy and Cell Biology, Albert-Ludwigs-University Freiburg, Freiburg 79104, Germany,
[2]Faculty of Biology, Albert-Ludwigs-University Freiburg, Freiburg 79104, Germany,
[3]Center for Basics in NeuroModulation (NeuroModul Basics), Medical Faculty, Albert-Ludwigs-University Freiburg, Freiburg 79104, Germany

*Corresponding author: Email: tanja.vogel@anat.uni-freiburg.de

†Arquimedes Cheffer, Marta Garcia-Miralles, and Esther Maier contributed equally.

The cortical plate (CP) is composed of excitatory and inhibitory neurons, the latter of which originate in the ganglionic eminences. From their origin in the ventral telencephalon, maturing postmitotic interneurons migrate during embryonic development over some distance to reach their final destination in the CP. The histone methyltransferase Disruptor of Telomeric Silencing 1-like (DOT1L) is necessary for proper CP development and layer distribution of glutamatergic neurons. However, its specific role on cortical interneuron development has not yet been explored. Here, we demonstrate that DOT1L affects interneuron development in a cell autonomous manner. Deletion of *Dot1l* in *Nkx2.1*-expressing interneuron precursor cells results in an overall reduction and altered distribution of GABAergic interneurons in the CP from postnatal day 0 onwards. We observed an altered proportion of GABAergic interneurons in the cortex, with a significant decrease in parvalbumin-expressing interneurons. Moreover, a decreased number of mitotic cells at the embryonic day E14.5 was observed upon *Dot1l* deletion. Altogether, our results indicate that reduced numbers of cortical interneurons upon DOT1L deletion result from premature cell cycle exit, but effects on postmitotic differentiation, maturation, and migration are likely at play as well.

Key words: DOT1L; Foxg1; GABAergic interneurons; Nkx2.1; parvalbumin.

Introduction

The development of the mammalian cerebral cortex follows an orchestrated set of events, including cell proliferation, migration, and differentiation. Through these events, cell types arise in a spatio-temporal-dependent manner, including the 2 main neuronal populations, namely the excitatory glutamatergic neurons and the inhibitory GABAergic interneurons. Glutamatergic neurons originate from the ventricular and subventricular zones of the pallium and migrate along radial glia cells to populate the cortical plate (CP) (Rakic 1995). Most of the cortical GABAergic interneurons arise from progenitors localized in the medial and caudal ganglionic eminences (MGE and CGE) in the subpallium (Lavdas et al. 1999; Flames et al. 2007), and smaller fractions derive from the lateral ganglionic eminence (Siddiqi et al. 2021) and the preoptic area (POA) (Gelman et al. 2009). Interneurons migrate tangentially into the cerebral cortex, where they switch to radial migration until they reach their final destination in specific cortical layers (Lavdas et al. 1999; Marín and Rubenstein 2001; Miyoshi and Fishell 2011). Although the cortical GABAergic interneurons, comprising 10%–15% of neurons, are less numerous than their glutamatergic counterparts (85%–90%) (Meyer et al. 2011), they are much more diverse regarding morphology, connectivity pattern, and electrophysiological properties (reviewed in Tremblay et al. 2016). Their integration into neuronal circuitries is crucial to ensure a proper cortical excitatory–inhibitory (E–I) balance and a normal brain functioning. Indeed, impairments in GABAergic neurotransmission and consequently altered E–I balance are implicated in many neurological and psychiatric conditions, including Alzheimer's disease, epilepsy, schizophrenia, autism, depression, and mood disorders (reviewed in Nahar et al. 2021; Prévot and Sibille 2021; Ruden et al. 2021). Therefore, information on the cues that govern the appropriate generation, migration, lamination, and circuitry integration of GABAergic interneurons gives insight into disease mechanisms and opens avenues for the development of treatments. In this sense, it has already been shown how transcription factors, cell adhesion molecules, extracellular matrix components, and chemoattractive and repulsive factors guide the generation, migration, and allocation of GABAergic interneurons in the developing cortex (Liodis et al. 2007; Nóbrega-Pereira et al. 2008; Wester et al. 2019; Limoni et al. 2021).

In addition to the molecules mentioned above, there is an increasing body of evidence showing that epigenetic control of gene expression plays an important role in the development of the central nervous system (CNS) (Juliandi et al. 2010; MuhChyi et al. 2013). Our group has investigated the involvement of the Disruptor of Telomeric Silencing 1-like (DOT1L), a highly conserved histone methyltransferase mediating histone H3 methylation at position lysine 79 (H3K79me), in neuronal differentiation (Büttner et al. 2010; Roidl et al. 2016; Bovio et al. 2019; Franz et al. 2019;

Received: January 28, 2023. **Revised:** July 10, 2023. **Accepted:** July 11, 2023

Ferrari et al. 2020; Gray de Cristoforis et al. 2020). We demonstrated that the loss of DOT1L in forebrain progenitors impairs cortical and hippocampus development. *Dot1l* conditional knockout (*Dot1l* cKO) results in a decreased progenitor pool owing to premature cell cycle exit and neuronal differentiation. DOT1L also affects the cell fate determination and layer distribution of upper and deep layer (UL and DL) neurons since the *Dot1l* deficiency leads to decreased numbers of UL neurons and aberrant distribution of DL neurons in the CP (Franz et al. 2019).

The broad expression of DOT1L in the CNS makes it likely that *Dot1l* deletion not only affects the glutamatergic lineage but also interferes with the development of GABAergic neurons. In fact, we demonstrated that *Dot1l* is necessary for the generation and migration of GABAergic interneurons in the developing spinal cord (Gray de Cristoforis et al. 2020). Furthermore, H3K79me2 marks deposited by DOT1L in the chromatin of GABAergic medium spiny neurons mediate stress response and susceptibility to depression-like behaviors in a mouse model. Notably, intraperitoneal injection of a DOT1L inhibitor reversed the social impairments associated with the depressive phenotype in these mice (Kronman et al. 2021).

Despite emerging evidence, it is not reported as of yet whether and how DOT1L is involved specifically in the development of cortical GABAergic interneurons. Here, we employed bulk RNA sequencing together with histological methods on two different *Dot1l* cKO mice, using either Forkhead box G1 (Foxg1)-cre or Nkx2.1-cre driver lines, to reveal the DOT1L effects on interneuron development. We show that *Dot1l* deletion impairs the embryonic development of GABAergic interneurons. Specifically, in MGE-derived interneurons, we observed sustained effects on the parvalbumin (*Pvalb*) expression fraction that exhibited postnatal reduction. Our transcriptomic data and lineage tracing of *Nkx2.1* expressing interneurons suggest altered proliferation, postmitotic differentiation, maturation, and migration as possible underlying mechanisms.

Material and methods

Detailed and extended information on material and methods used in this study are found in the supplementary material.

Animals

Foxg1-cre (Hébert and McConnell 2000) were mated with floxed *Dot1l* animals. Animals with the genotype Foxg1$^{cre/+}$;Dot1l$^{flox/flox}$ (cKO) were analyzed in comparison with littermate controls with Foxg1$^{+/+}$:Dot1l$^{flox/+}$ or Foxg1$^{+/+}$:Dot1l$^{flox/flox}$. NK2 Homeobox 1 (Nkx2.1)-cre animals (Xu et al. 2008; JAX #008661) were initially mated with either a R26R(EYFP) line (Srinivas et al. 2001; JAX #006148) or a R26R (Sun1-GFP) line (Mo et al. 2015; JAX #021039) to generate Nkx2.1-cre/R26R (EYFP) and Nkx2.1-cre/R26R (Sun1-GFP) animals, respectively, which were subsequently mated with floxed *Dot1l*. For immunostaining GFP-positive cells at E14.5 and E18.5, animals with the genotype Nkx2.1$^{cre/+}$/R26R (Sun1-GFP);Dot1l$^{flox/flox}$ (cKO) were analyzed in comparison with littermate controls with Nkx2.1$^{+/+}$/R26R(Sun1-GFP); Dot1l$^{flox/+}$, Nkx2.1$^{+/+}$/R26R (Sun1-GFP); Dot1l$^{flox/flox}$, Nkx2.1$^{cre/+}$/R26R (Sun1-GFP); Dot1l$^{+/+}$ or Nkx2.1$^{cre/+}$/R26R (Sun1-GFP); Dot1l$^{flox/+}$. For other experiments, animals with the genotype Nkx2.1$^{cre/+}$/R26R (EYFP); Dot1l$^{flox/flox}$ (cKO) were analyzed in comparison to littermate controls with Nkx2.1$^{+/+}$/R26R(EYFP); Dot1l$^{flox/+}$, Nkx2.1$^{+/+}$/R26R(EYFP); Dot1l$^{flox/flox}$, Nkx2.1$^{cre/+}$/R26R(EYFP); Dot1l$^{+/+}$ or Nkx2.1$^{cre/+}$/R26R(EYFP);Dot1l$^{flox/+}$. Animal experiments were approved by the animal welfare committees of the University of Freiburg and local authorities (G16/11 and G21/0182).

Immunostaining, imaging, and quantification

A detailed protocol is described in the supplementary material. The following first and secondary antibodies were used: anti-cleaved caspase 3 (rabbit; 1:200; Cell Signaling; 9664S), anti-GFP (chicken; 1:500; Abcam; ab13970), anti-BrdU (sheep; 1/100; Abcam; ab1893), anti-Ki67 (rabbit; 1:250; Abcam; ab15580), anti-SOX6 (rabbit; 1:50; Santa Cruz; sc-20,092), anti-PHH3 (rabbit; 1:200; Abcam; ab5176), antirabbit Alexa 594 (donkey; 1:500; Thermo Fisher; R37119), anti-rabbit Alexa 488 (donkey; 1:500; Thermo Fisher; A27034), anti-chicken Alexa 488 (goat; 1:500; Thermo Fisher; A78948), and anti-sheep Cy3 (donkey; 1:500; Jackson ImmunoResearch; AB 2315778).

Single molecule fluorescent in situ hybridization, imaging, and quantification

A detailed protocol is described in the supplementary material. The following single molecule fluorescent in situ hybridization (smFISH) probes and fluorophores were used: *Plcdx3*-C3 probe (mouse; ACD; 498,091) with Opal 570 fluorophore (1:1500); *Phlda1*-C2 probe (mouse; ACD; 593,561) with Opal 570 fluorophore (1:1500); *Pvalb*-C1 probe (mouse; ACD; 421,931) with Opal 520 fluorophore (1:1000); eGFP-C2 (mouse; ACD; 400,281) with Opal 570 fluorophore (1:1000); and somatostatin (*Sst*)-C3 probe (mouse; ACD; 404,631) with Opal 650 fluorophore (1:1000).

In situ hybridization, imaging, and quantification

A detailed protocol is described in the supplementary material. Probes for in situ hybridization (ISH) were made by cloning PCR products into pGemTeasy (Promega). Sections were incubated with the probes, and after blocking and incubation with Anti-DIG-AP (Roche), sections were developed and mounted. Bright field images were obtained using an Axioplan M2 microscope (Zeiss). Quantification was done with Fiji-ImageJ. The ISH probe sequences were obtained from the following sources: *Nkx2.1* (Addgene; 15,540); *Lhx6* (Allen Brain Atlas; Experiment #100047358); *Nr2f2* (Allen Brain Atlas; Experiment #100057642); *Prox1* (Addgene; 87,129), *Sp8* (Kawakami et al. 2004); and *Sst* (Asgarian et al. 2019).

RNA sequencing and bioinformatics analysis

A detailed protocol is described in the supplementary material. Libraries from total RNA were prepared using the NEBNext Ultra RNA Library Prep Kit for Illumina. The procedure included depletion of rRNA prior double-stranded cDNA synthesis and library preparation. Samples were sequenced on Illumina HiSeq3000 as paired-end 75-bp reads. Quality control, trimming, mapping of the RNA sequencing fastq files, and generation of gene-level counts was done on the Galaxy platform (Afgan et al. 2022). Differential expression analysis was done using DESeq2 (1.34.0) on R (4.2.0) on the count matrix output from featurecounts (Love et al. 2014). GO term enrichment analyses were done using clusterProfiler (4.2.2) (Wu et al. 2021). Visualizations of volcano plots and heatmaps were done using EnhancedVolcano (1.12.0) and pheatmap (1.0.12) packages, respectively (Kolde 2019; Blighe and Rana 2022).

Statistical analyses

For statistical analysis, an unpaired, 2-tailed Student's *t*-test with Welch's correction was performed with GraphPad Prism software (version 9.1.1).

Results

Dot1l deletion in the Foxg1-cre lineage impairs cortical interneuron development

Foxg1 is involved in interneuron development, and we used the recently described Foxg1^{cre} Dot1l cKO mouse line to explore whether DOT1L affects the development of GABAergic interneurons (Franz et al. 2019). Transcriptomic analysis of the dorsal telencephalon of cKO (Foxg1$^{cre/+}$Dotl1$^{flox/flox}$) and control (Foxg1$^{+/+}$Dotl1$^{flox/+}$) mice at E14.5 revealed altered expression of 2,106 genes in total (Franz et al. 2019). We manually curated current literature on the interneuron development to short-list genes expressed by interneurons (Wonders and Anderson 2006; Faux et al. 2012; Chen et al. 2017; Mayer et al. 2018; Mi et al. 2018; Asgarian et al. 2022), which summed up to 534 genes (Supplementary Table 2). 86 of these interneuron genes were differentially expressed upon *Dot1l* cKO (*P*. adj. value < 0.05), with both increased and decreased expression levels when compared to control mice (Fig. 1A–C). Notably, the GABAergic MGE markers *Lhx6*, *Sox6*, *Sst*, and *Npy* decreased significantly upon *Dot1l* deletion, while the CGE markers *Calb1*, *Htr3a*, and *Nr2f2* exhibited a milder decrease in their expression, suggesting that the MGE-derived interneuron lineages were more affected (Fig. 1C). Functional GO term enrichment analysis indicated that genes impacting the maturation, migration, and terminal differentiation of interneurons were altered upon DOT1L deletion (Fig. 1D).

Foxg1 is expressed in the dorsal and ventral telencephalon (vT), and its cre-driver activity resulted in the loss of *Dot1l* transcription in both regions (Supplementary Fig. S1A). Taking this broad expression and the presence of interneurons in both regions into account, we validated the expression of selected genes that impact interneurons separately in the two regions at E14.5 using qRTPCR (Supplementary Fig. S1B–H). Based on the developmental stage in which the interneuron marker genes are expressed (Wonders and Anderson 2006), we categorized the markers according to cell cycle exit, interneuron specification, immature or migrating interneurons, and interneuron subtypes. Genes that did not fall into these categories were considered as other interneuron markers. In line with the transcriptomic analysis (Fig. 1A), we observed an altered expression of several interneuron markers in both dorsal telencephalon (dT) and vT. Notably, interneuron markers transcribed in immature interneurons, namely *Lhx6*, *Cux2*, *Lmo1*, and *Sox6*, decreased in both regions (Supplementary Fig. S1E), whereas the transcriptional decrease of markers depicting migrating interneurons or interneuron subtypes only significantly decreased in the dorsal telencephalon, namely *Nrp1*, *Hrt3a*, *Erbb4*, *Sst*, *Nxph1*, and *Npy* (Supplementary Fig. S1F and G). The altered expression levels of these marker genes indicated that (i) Foxg1^{cre} Dot1l cKO affected the MGE-derived Nkx2.1 SST/NPY/PVALB lineage, and that (ii) the generation and early specification of interneurons were probably less affected than subsequent maturing stages of development. Confirming the hypothesis of a compromised development of the MGE-derived interneurons was the decreased expression of *Lhx6* and *Sox6*, which is in contrast to the *Dlx* family members (Supplementary Fig. S1D and E). While the decreased expression of genes characterizing the MGE-derived lineage was prominent, we observed an increased expression of CGE-lineage marker genes *Calb2* and *Ache* in the vT (Supplementary Fig. S1G). To gain insight into one possible molecular mechanism by which DOT1L regulates the interneuron development, we inspected the enrichment of H3K79me2 marks at the different genes expressed by interneurons from a data set derived from the E14.5 wild-type dorsal telencephalon (Supplementary Fig. S2A–F) (Franz et al. 2019). In this set of candidate genes, we identified several genes that were marked by H3K79me2 and which, therefore, could be directly controlled by DOT1L's enzymatic activity. We found the strongest enrichment of genes carrying H3K79me2 in immature interneuron marker genes (Supplementary Fig. S2C). Notably, this state during interneuron development also showed a decreased expression of the respective markers in the transcriptome. Using ISH or immunohistochemistry, we observed in vivo reduced expression of *Nkx2.1*, *Lhx6*, *Sst*, *Nr2f2*, *Sp8*, and SOX6 (Fig. 2A–F). We counted significantly reduced cell numbers for *Sst* (Fig. 2C and G), but not for SOX6 (Fig. 2F and H), in the cerebral cortex of *Dot1l* cKO mice at E18.5 compared to the control group. ISH of the MGE marker *Nkx2.1* and of the CGE markers *Prox1* and *Sp8* at the earlier developmental stages E12.5 and E14.5 retrieved positive signals in the expected location (Supplementary Fig. S3). This finding indicated that the alterations observed at E18.5 were not due to gross anatomical misspecification of the MGE and CGE but were more likely due to the proliferation or maturation defects upon *Dot1l* deletion. Taken together, the data suggested that proper expression of *Dot1l* is necessary for the correct development of MGE- and CGE-derived interneurons.

Dot1l deletion in the Nkx2.1-cre lineage alters transcriptional programs of cortical interneurons

Foxg1 is broadly expressed within both the ventral and dorsal telencephalon (Dou et al. 1999), and the concomitant *Dot1l* deficiency using Foxg1-cre could thus have cell autonomous and nonautonomous effects on the developing interneurons. In addition, Foxg1^{cre} Dot1l cKO mice die around birth, hampering detailed examination of the interneuron classes that express relevant markers, e.g. PVALB, postnatally. Furthermore, *Foxg1* haploinsufficiency itself affects forebrain development (Shen et al. 2006; Miyoshi et al. 2021). In fact, *Foxg1*-haploinsufficient animals also exhibit dysregulated expression of interneuron marker genes (Franz et al. 2019), from which a substantial portion was shared with Foxg1^{cre} Dot1l cKO animals in the dorsal telencephalon (Supplementary Fig. S2G and H). Discrimination between the contributions of the *Foxg1* haploinsufficiency and the *Dot1l* deletion to the impaired interneuron development is thus difficult. We therefore used the Nkx2.1-cre as driver line to focus our study on cell autonomous effects of DOT1L in the interneuron lineage that derives mainly from the MGE and POA (Gelman et al. 2009). Since *Dot1l* expression reaches a peak at E14.5 in the developing telencephalon (Franz et al. 2019), we confirmed first by qRTPCR that *Dot1l* expression reduced in the vT of E14.5 cKO (Nkx2.1$^{cre/+}$Dotl1$^{flox/flox}$) compared to control (Nkx2.1$^{+/+}$Dotl1$^{flox/+}$) animals (Fig. 3A). Subsequently, we performed RNA sequencing for both ventral and dorsal telencephalon separately. RNA sequencing analysis of the vT from the control and cKO mice at E14.5 revealed 747 differentially expressed genes (DEGs) (*P* adj. value < 0.05), of which we classified 67 as the interneuron marker genes (Fig. 3B and C). From the dorsal telencephalon, we retrieved only 17 DEGs (*P*. adj. value < 0.1), of which only 1 classified as interneuron marker gene upon applying our curated short list (Supplementary Fig. S4A–C), and 2 DEGs were shared between the dT and vT data sets (Supplementary Fig. S4D). Focusing on the 67 DEGs from the vT, we found both increased and decreased expressions (Fig. 3D). Functional GO term enrichment analysis revealed an increased expression of genes associated to processes characteristic for postmitotic neurons, such as regulation of membrane potential,

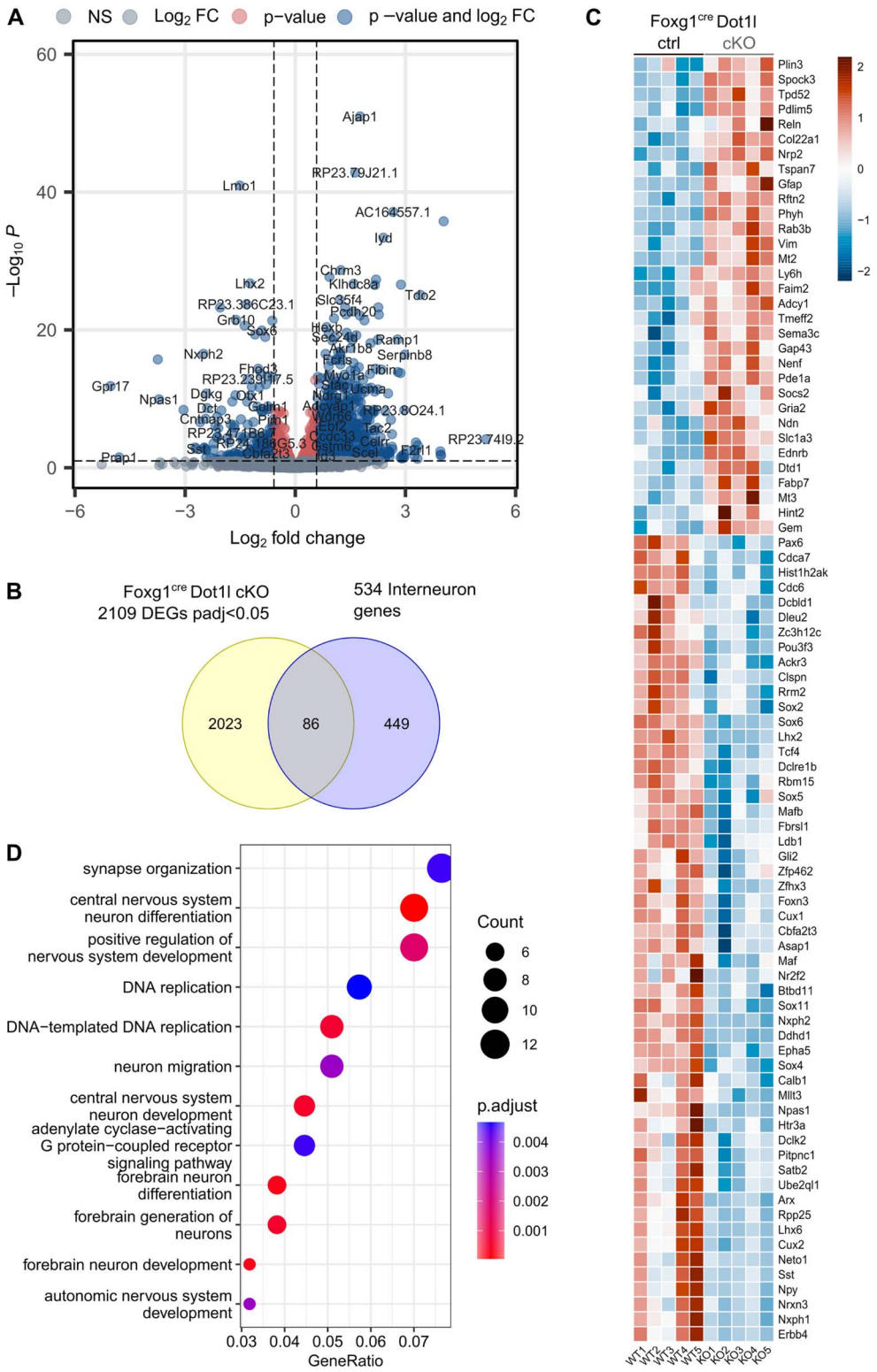

Fig. 1. *Dot1l* deletion in the Foxg1-cre lineage impairs cortical interneuron development. A) Volcano plot displaying differentailly expressed genes (DEGs) in the dorsal telencephalon of Foxg1^{cre} Dot1l cKO animals compared to controls at E14.5 using RNA sequencing. The *y*-axis corresponds to the adjusted *P*-value and the *x*-axis displays the $\log_2$fold change ($\log_2$FC). Transcripts with insignificant adjusted *P*-values ($P > 0.05$) below dashed horizontal line. Transcripts with differential expression of less than $\pm\log_2$ (0.5) and transcripts with differential expression of more than $\pm\log_2$ (0.5) are separated by the two vertical dashed lines. Positive $\log_2$FC represents increase; negative $\log_2$FC represents decrease in expression upon *Dot1l* deletion. B) Venn diagram of DEGs in dorsal telencephalon of Foxg1^{cre} Dot1l cKO animals at E14.5 that are known to be interneuron gene markers. C) Heatmap of 86 genes at the intersection in (B). DEGs with increased and decreased expressions are represented in red or blue, respectively. Scale shows scaled VST normalized gene counts. Data represent sex- and batch-corrected gene expression in forebrain of Foxg1^{cre} Dot1l control ($n = 5$) and cKO ($n = 5$) animals. D) Dotplot of GO term enrichment analysis of DEGs in Foxg1^{cre} Dot1l cKO mice depicting the top 12 significantly enriched biological processes. Total number of genes per group and adjusted *P*-values are indicated on the right and gene ratios are on the *x*-axis. Blue depicts the least significantly enriched pathway, and red depicts the most significantly enriched pathway.

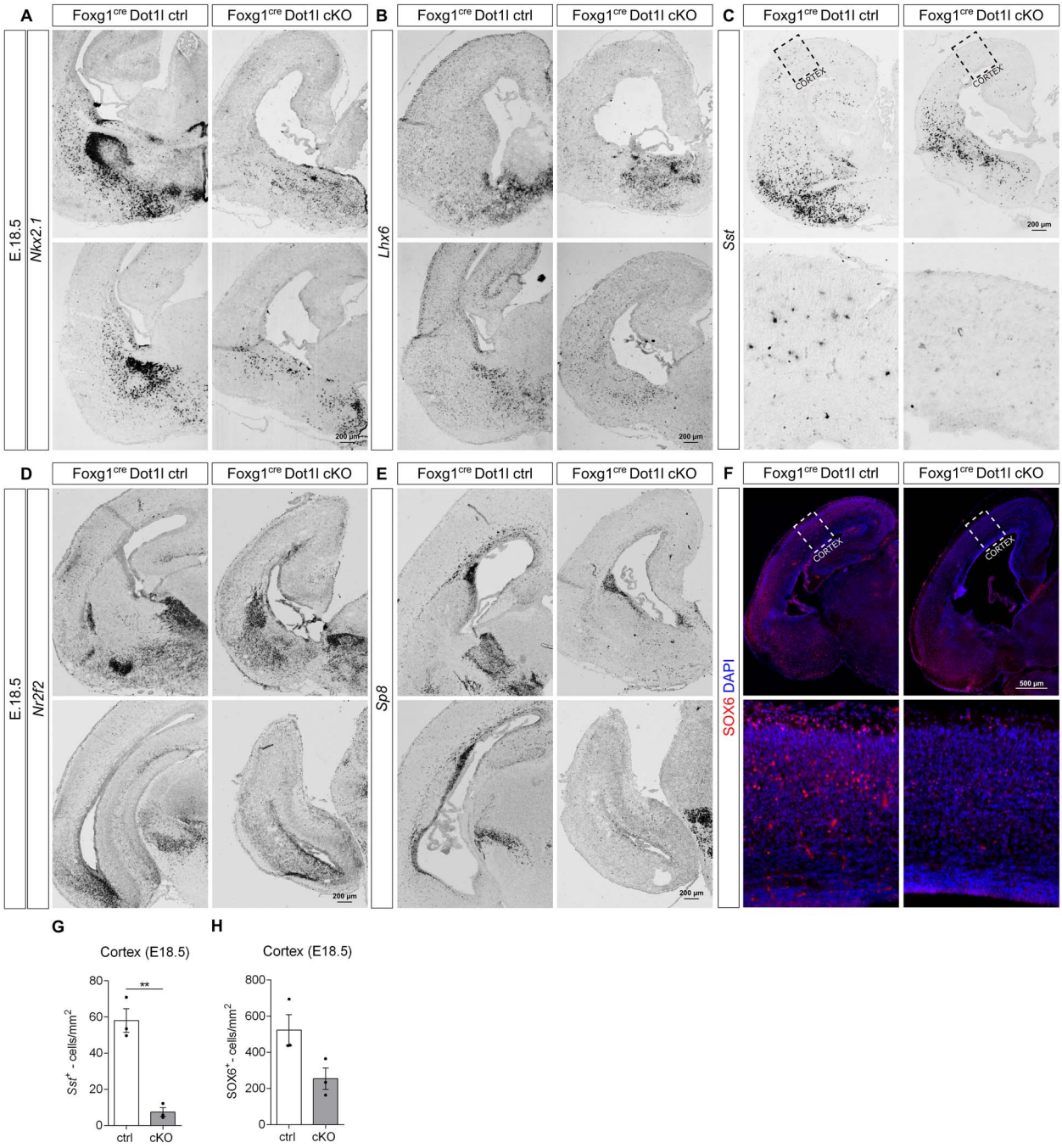

Fig. 2. *Dot1l* is necessary for proper development of MGE- and CGE-derived interneurons. A–E) Representative images of ISH of embryonic brain sections using A) *Nkx2.1*, B) *Lhx6*, C) *Sst*, D) *Nr2f2*, and E) *Sp8* antisense probes at embryonic stage E18.5. *Nkx2.1*, $n = 3$–4; *Lhx6*, *Nr2f2*, and *Sp8*, $n = 1$ (Foxg1^{cre} Dot1l ctrl and cKO animals). Scale bars: 200 μm. F) Representative images of immunostaining of E18.5 forebrain sections for SOX6 (red) and DAPI (blue); $n = 3$ (Foxg1^{cre} Dot1l ctrl and cKO animals). Scale bars: 500 μm. G) Quantification of *Sst*-expressing cells in the cerebral cortex of Foxg1^{cre} Dot1l cKO animals at E18.5. Data are represented as the mean ± SEM; $n = 3$ (Foxg1^{cre} Dot1l ctrl and cKO animals); $^{**}P < 0.01$ by unpaired, 2-tailed Student's *t*-test with Welch's correction. H) Quantification of SOX6-expressing cells in the cortex of Foxg1^{cre} Dot1l cKO animals at E18.5. Data are represented as the mean ± SEM; $n = 3$ (Foxg1^{cre} Dot1l ctrl and cKO animals); $P > 0.05$ by unpaired, 2-tailed Student's *t*-test with Welch's correction.

neurotransmitter transport, and synapse organization. Cell cycle-related terms, for instance, cell cycle phase transition, DNA replication, or neural precursor cell proliferation, were enriched in genes with decreased expression (Fig. 3E). Accordingly, among DEGs with decreased expression upon *Dot1l* deletion, we observed an enrichment of genes expressed in progenitor cells, whereas several markers for postmitotic neurons showed an increased expression (Supplementary Fig. S4E and F). Among the genes with decreased expression, we also observed the key regulatory transcription factors *Arx*, *Dlx1/2*, *Foxg1*, *Ldb1*, *Nkx2.1*, and *Sp9* (Fig. 3D). The decreased *Foxg1*, *Ldb1*, *Nkx2.1*, and *Sp9* expressions were further validated by means of qRTPCR (Fig. 3F). Inspection of the H3K79me2 distribution at these genes rendered these interneuron markers as potential, direct DOT1L-regulated target genes (Supplementary Fig. S2B and C, Fig. 3G). Compared to the Foxg1^{cre} Dot1l cKO, we identified 162 common target genes with the Nkx2.1^{cre}-mediated cKO, 16 of which classified as interneuron markers (Supplementary Fig. S4G and H). Shared

DEGs between both mouse lines contained a set of genes with opposing expression changes, but around 2/3 of DEGs decreased in both models. Compromised expression of instructors of interneuron development affected in both cKO models included *Arx*, *Lmo1*, *Sox1/2*, *Tcf4*, and *Zswim5* (Supplementary Fig. S4H). Together, our data indicated that DOT1L is implicated in the proper embryonic development of interneurons from the *Nkx2.1* lineage by regulating the expression of key transcription factors.

Dot1l deletion in the Nkx2.1-cre lineage reduces the number of cortical interneurons

We next explored the expression of interneuron markers by histological methods in vivo. ISH at E14.5 and E18.5 revealed a reduced expression of *Nkx2.1* (Supplementary Fig. S5A and C). As expected, the *Nkx2.1* downstream effector *Lhx6* (Sandberg et al. 2016) also decreased in its expression at both developmental time points (Supplementary Fig. S5B and D). The CGE markers *Nr2f2* and *Prox1* (both at E14.5 and E18.5) and the dorsal MGE marker *Nkx6.2* (at E14.5) neither showed differential expression in the transcriptome nor striking different staining patterns using ISH, supporting the specificity of the cKO in the *Nkx2.1* lineage (Supplementary Fig. S6A–E).

For gaining further insight into how the observed transcriptional changes upon *Dot1l* deletion would impact the *Nkx2.1* lineage-derived interneurons (here, simply named *Nkx2.1* interneurons), we characterized these interneurons at different developmental stages: (i) at embryonic day E14.5, when most of the cells in the MGE are neuronal progenitors; (ii) at embryonic day E18.5, when postmitotic interneurons are still migrating to the cortex; (iii) at postnatal day 0 (P0), when the interneurons completed their migration to the cerebral cortex; and (iv) at postnatal day 21 (P21), when lamination as well as circuit integration and refinement are completed (Lim et al. 2018). To this end, we traced the *Nkx2.1* interneurons using either a ROSA26-YFP or a ROSA26-SUN1-GFP reporter mouse line crossed with the Nkx2.1^{cre} Dot1l line. A statistically significant decrease in the number of MGE-derived interneurons was observed in the cortex (757.10 ± 18.03 cells/mm^2 vs. 1011 ± 39.64 cells/mm^2; $^{**}P < 0.01$) of cKO mice at P0, but not at E14.5 and E18.5, when compared to control animals (Fig. 4A–F). The striatum of cKO mice also showed decreased numbers of interneurons (246.00 ± 14.72 cells/mm^2 vs. 457.70 ± 40.14 cells/mm^2; $^{**}P < 0.01$) at P0 when compared to control animals (Fig. 4G and H). Upon surveying the laminar distribution of *Nkx2.1* interneurons, we observed increased numbers in the upper third of the CP at E14.5 (Fig. 4B), decreased numbers of GFP-positive cells in the MZ at E18.5 (Fig. 4D), and at P0 decreased numbers of GFP-labeled interneurons in MZ, but increased numbers in the lower half of the cortex (bins 5–8; bin 1: MZ, bin 10: VZ) (Fig. 4F). Together, the developmental distribution of *Nkx2.1* interneurons upon *Dot1l* deletion suggested a premature invasion of GABAergic neurons in the CP and a depletion of the pial migratory stream. In accordance with an altered migratory pattern of interneurons upon *Dot1l* deletion, we observed that genes related to cell-to-cell interactions, including *Ackr3*, *Epha3*, *Epha4*, *Efnb1*, and *Efnb3*, as well as genes encoding for chemokines, for instance, *Sema5b*, *Sema6a*, and *Cxcl14* were differentially expressed upon *Dot1l* deletion (Supplementary Fig. S4I). However, a closer inspection of the subpallial-pallial boundary (SPB) of the control and cKO animals at E14.5, a time point where we observed increased numbers of interneurons in CP and the tangential migration to the cortex is high, did not indicate that more interneurons crossed the SPB upon *Dot1l* deletion (Supplementary Fig. S7A and B). We also did not have indication that, instead of using the pial migratory route, *Nkx2.1* interneurons would be rerouted to the intermediate zone during tangential migration (Fig. 4A and C). As these findings made an increased migration from the MGE to the cortex as a sole mechanism for the increased number of interneurons in the CP at P0 unlikely, we hypothesized that an altered migratory behavior of *Nkx2.1* interneurons would go in hand with a premature differentiation and probably depletion of progenitors. This assumption was supported by DEGs associated with progenitor proliferation or differentiation (Supplementary Fig. S4E and F).

Taking these observations together, we hypothesized that the increase in *Nkx2.1* interneurons at P0 in the CP of *Dot1l* deletion animals might reflect a transient developmental state and that overall fewer interneurons, also in regard to their representation in the different layers, would be present at a later stage. To support our hypothesis, we performed smFISH for *Pvalb* and *Sst* as well as for GFP at P21, which allowed the determination of overall numbers and further discrimination among *Pvalb*-expressing, *Sst*-expressing, and *Pvalb/Sst*-negative interneurons in the total *Nkx2.1* interneuron population, respectively (Fig. 5A and B). As expected, the number of *Nkx2.1*-lineage interneurons expressing GFP in the cerebral cortex of cKO animals was significantly reduced (58.17 ± 8.05 cells/mm^2 vs. 86.99 ± 7.47 cells/mm^2; $^{*}P < 0.05$) (Fig. 5C). Within the different subfractions, we observed significantly less GFP/*Pvalb*-expressing interneurons in the cortex of cKOs compared to controls (14.27 ± 2.38 cells/mm^2 vs. 32.45 ± 4.65 cells/mm^2; $^{*}P < 0.05$) (Fig. 5D), but both GFP/*Sst* (36.22 ± 4.43 cells/mm^2 vs. 41.17 ± 4.86 cells/mm^2; $P > 0.05$) (Fig. 5E) and the remaining GFP-expressing interneurons, being negative for both *Pvalb* and *Sst*, did not change (7.67 ± 1.89 cells/mm^2 vs. 13.37 ± 5.31 cells/mm^2; $P > 0.05$) (Fig. 5F). We also compared the laminar distribution of all GFP-expressing interneurons and the two GFP-positive subfractions coexpressing either *Pvalb* or *Sst* to discard any confounding effect coming from reduced cell densities. The upper half of the cortex contained reduced numbers of GFP-expressing interneurons as well as reduced numbers of *Pvalb*-coexpressing *Nkx2.1* interneurons (Fig. 5C and D). *Sst*-coexpressing interneurons did not have an altered laminar distribution (Fig. 5E). The number of *Sst*-positive interneurons was also not changed significantly at P0 (Supplementary Fig. S8). Thus, the significant decrease in the GFP-expressing interneurons as observed in P21 upon *Dot1l* deletion seemed to be mainly caused by the reduction in the *Pvalb*-expressing subfraction (Fig. 5G). We also supported by analyzing P21 our hypothesis that the increased numbers of *Nkx2.1* interneurons in the CP at P0 was a transient state.

Since PVALB expression is not detectable at embryonic and early postnatal stages, we used two markers for immature *Pvalb*-expressing interneurons, *Phlda1* and *Plcxd3* (Mayer et al. 2018), to assess whether immature *Pvalb* interneurons were already reduced at the embryonic development stages E14.5 and E16.5 and at the postnatal stage P0 (Supplementary Fig. S9A). We did not observe statistically significant changes in the cell numbers for *Phlda1* and *Plcxd3* expression.

We further assessed whether the reduction of *Nkx2.1* interneurons, most likely affecting the *Pvalb*-expressing fraction, upon *Dot1l* cKO, would be caused by an increased apoptosis of MGE progenitors at E14.5 and E18.5. We did not observe increased numbers of cells expressing aCASP3 in cKO mice, rendering it unlikely that apoptosis of MGE progenitors upon *Dot1l* cKO contributed massively to the decreased numbers of interneurons

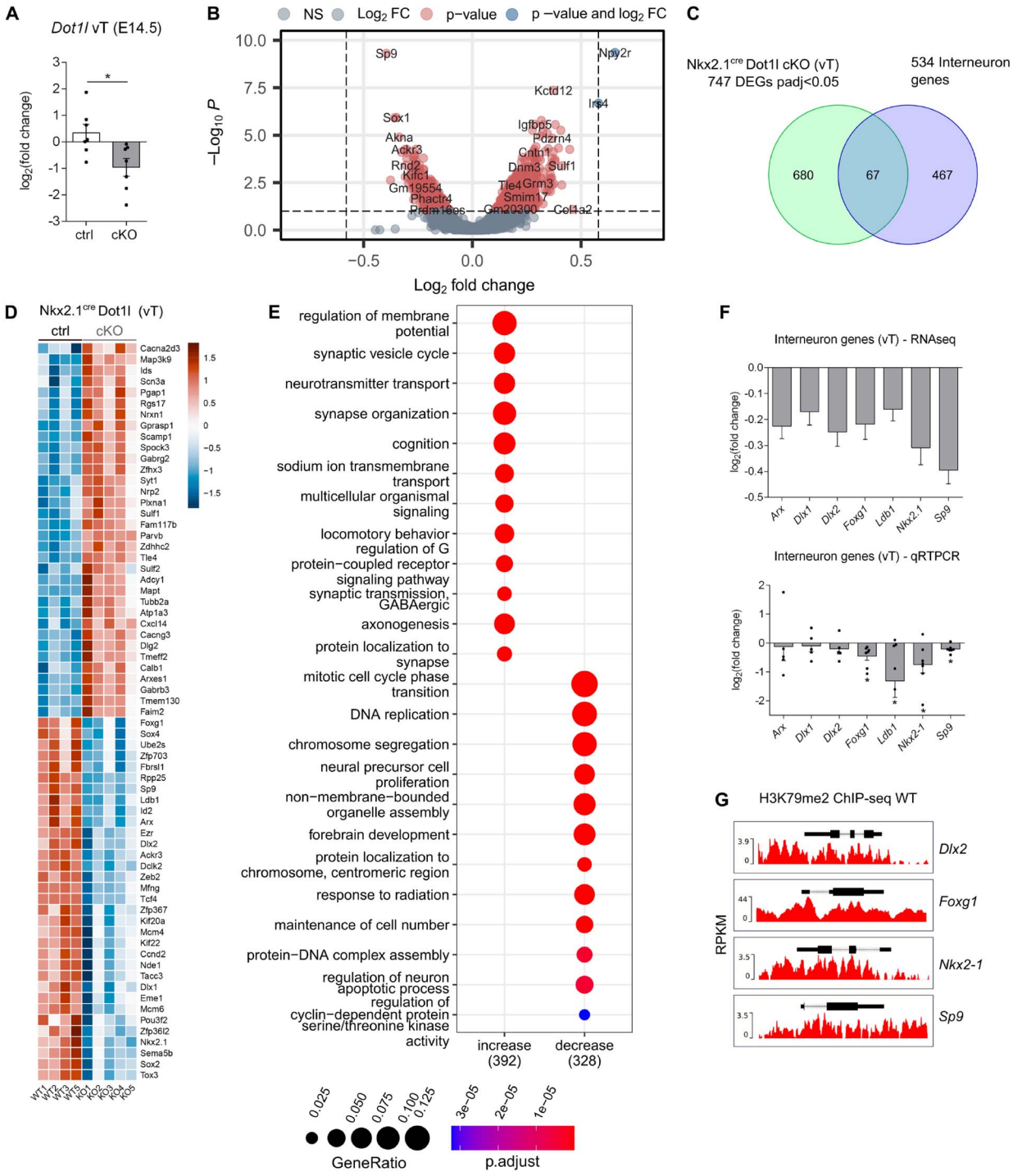

Fig. 3. *Dot1l* deletion in the Nkx2.1-cre lineage impairs cortical interneuron development. A) qRTPCR of *Dot1l* expression in cKO versus control in the vT. Data are represented as the mean + SEM; $n = 7$ (Nkx2.1^{cre} Dot1l ctrl and cKO animals); *$P < 0.05$ by unpaired, 2-tailed Student's *t*-test with Welch's correction. B) Volcano plot displaying DEGs in the vT of Nkx2.1^{cre} Dot1l cKO animals compared to controls at E14.5. The *y*-axis corresponds to the adjusted *P*-value and the *x*-axis displays the $\log_2$FC. Transcripts with insignificant adjusted P-values ($P > 0.05$) below dashed horizontal line. Transcripts with differential expression of less than ±log2 (0.5) and transcripts with differential expression of more than ±log2 (0.5) are separated by the two vertical dashed lines. Positive $\log_2$FC represents increase and negative $\log_2$FC represents decrease in expression upon *Dot1l* deletion. C) Venn diagram showing the intersection of DEGs in vT of Nkx2.1^{cre} Dot1l cKO animals at E14.5 and genes classified as interneuron marker genes. D) Heatmap of 67 intersected genes in (C). DEGs with increased or decreased expression are represented in red or blue, respectively. Scale shows scaled VST normalized gene counts. Data represent sex- and batch-corrected gene expression in vT of Nkx2.1^{cre} Dot1l control ($n = 4$) and cKO ($n = 5$) animals. E) Dotplot of differential GO term enrichment analysis of increasing and decreasing DEGs in Nkx2.1^{cre} Dot1l cKO mice. Gene ratios and adjusted *P*-values are indicated at the right, and total number of genes per group is shown on the *x*-axis. Blue depicts the least significantly enriched pathway, and red depicts the most significantly enriched pathway. F) Upper panel: RNA sequencing results ($\log_2$FC) of Nkx2.1^{cre} Dot1l cKO animals for *Arx*, *Dlx1*, *Dlx2*, *Foxg1*, *Ldb1*, *Nkx2.1*, and *Sp9*. Lower panel: qRTPCR validation for the same genes in cKO versus control in the vT. Data is represented as the mean + SEM; $n = 5$–7 (Nkx2.1^{cre} Dot1l ctrl and cKO animals); *$P < 0.05$ by unpaired, 2-tailed Student's *t*-test with Welch's correction. G) ChIP-seq results of H3K79me2 levels at *Dlx2*, *Foxg1*, *Nkx2.1*, and *Sp9* genes in E14.5 wild-type cerebral cortex, a set of candidate genes, which also decreased in expression in the vT in Nkx2.1^{cre} Dot1l cKO animals at E14.5 as revealed by RNA sequencing and shown in (D). Peaks indicate enrichment of H3K79me2 for genes with decreased expression.

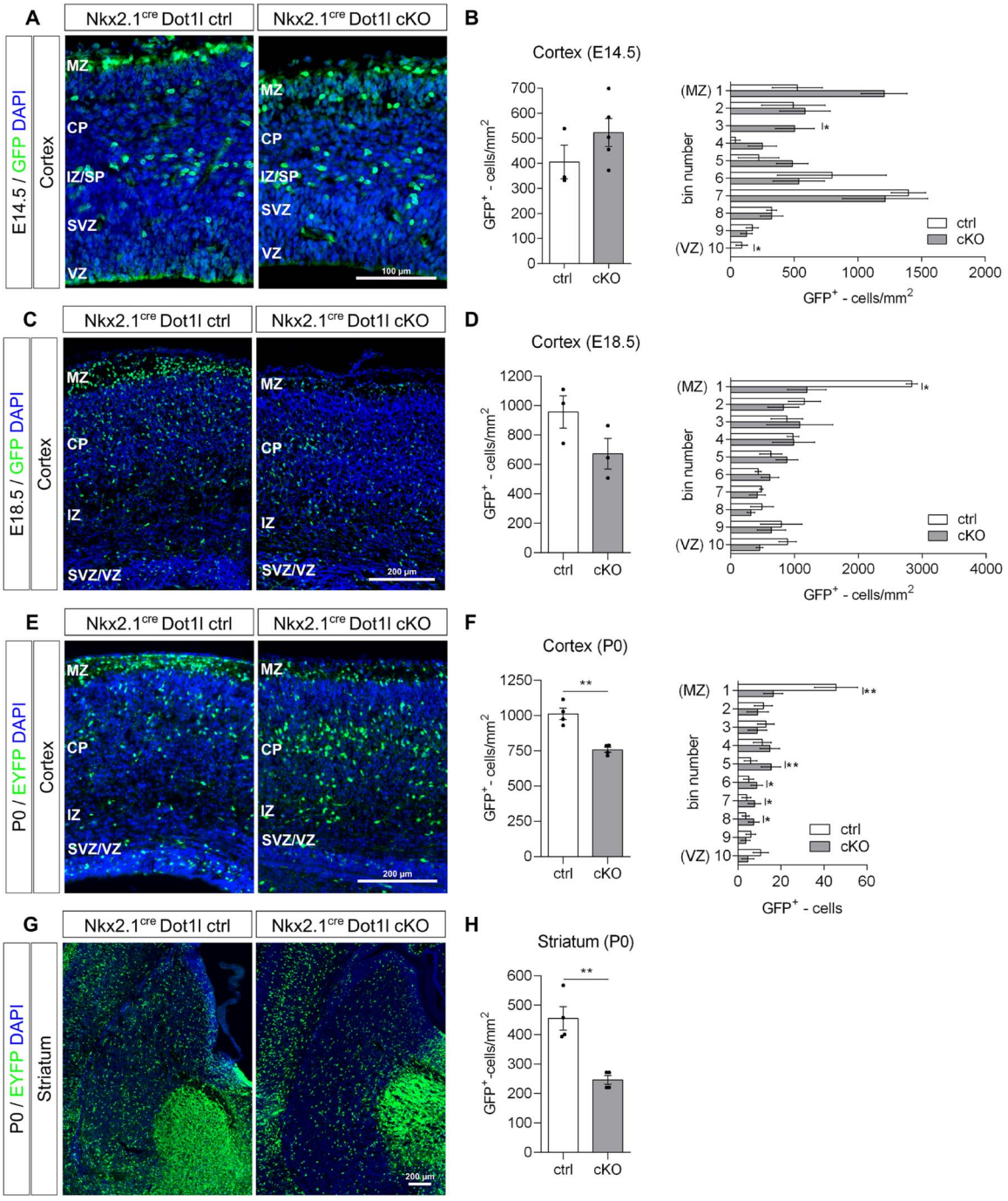

Fig. 4. *Dot1l* deletion in the Nkx2.1-cre lineage reduces the number of cortical interneurons at different developmental stages. A) Representative images of immunostaining of embryonic (E14.5) forebrain sections for GFP (SUN1-GFP) (green) and DAPI (blue) in the cerebral cortex, $n = 4$–5 (Nkx2.1^{cre} Dot1l control and cKO animals). Scale bars: 100 μm. B) Quantification of total Nkx2.1-derived GABAergic interneurons (GFP$^+$ cells) in the E14.5 cortex and within each individual bin out of 10 bins spanning the entire cortex from VZ (bin 10) to the marginal zone (bin 1). Data are represented as the mean ± SEM; cortex and striatum: $n = 4$–5 (Nkx2.1^{cre} Dot1l ctrl and cKO animals); *$P < 0.05$ by unpaired, 2-tailed Student's *t*-test with Welch's correction. C) Representative images of immunostaining of embryonic (E18.5) forebrain sections for GFP (SUN1-GFP) (green) and DAPI (blue) in the cerebral cortex, $n = 3$ (Nkx2.1^{cre} Dot1l control and cKO animals). Scale bars: 200 μm. D) Quantification of total *Nkx2.1*-derived GABAergic interneurons (GFP$^+$ cells) in the E18.5 cortex and within each individual bin out of 10 bins spanning the entire cortex from VZ (bin 10) to the marginal zone (bin 1). Data are represented as the mean ± SEM; cortex and striatum: $n = 3$ (Nkx2.1^{cre} Dot1l ctrl and cKO animals); *$P < 0.05$ by unpaired, 2-tailed Student's *t*-test with Welch's correction. E) Representative images of immunostaining of postnatal (P0) forebrain sections for GFP (EYFP) (green) and DAPI (blue) in the cerebral cortex, $n = 4$ (Nkx2.1^{cre} Dot1l control and cKO animals). Scale bars: 200 μm. F) Quantification of total *Nkx2.1*-derived GABAergic interneurons (GFP$^+$ cells) in the postnatal cortex and within each individual bin out of 10 bins spanning the entire cortex from VZ (bin 10) to the marginal zone (bin 1). Data are represented as the mean ± SEM; cortex and striatum: $N = 4$ (Nkx2.1^{cre} Dot1l ctrl and cKO animals); **$P < 0.01$ by unpaired, 2-tailed Student's *t*-test with Welch's correction. G) Representative images of immunostaining of postnatal (P0) forebrain sections for GFP (EYFP) (green) and DAPI (blue) in the striatum, $n = 4$ (Nkx2.1^{cre} Dot1l control and cKO animals). Scale bars: 200 μm. H) Quantification of *Nkx2.1*-derived GABAergic interneurons (GFP$^+$ cells) in the postnatal cortex and striatum. Data are represented as the mean ± SEM; cortex and striatum: $n = 4$ (Nkx2.1^{cre} Dot1l ctrl and cKO animals); **$P < 0.01$ by unpaired, 2-tailed Student's *t*-test with Welch's correction.

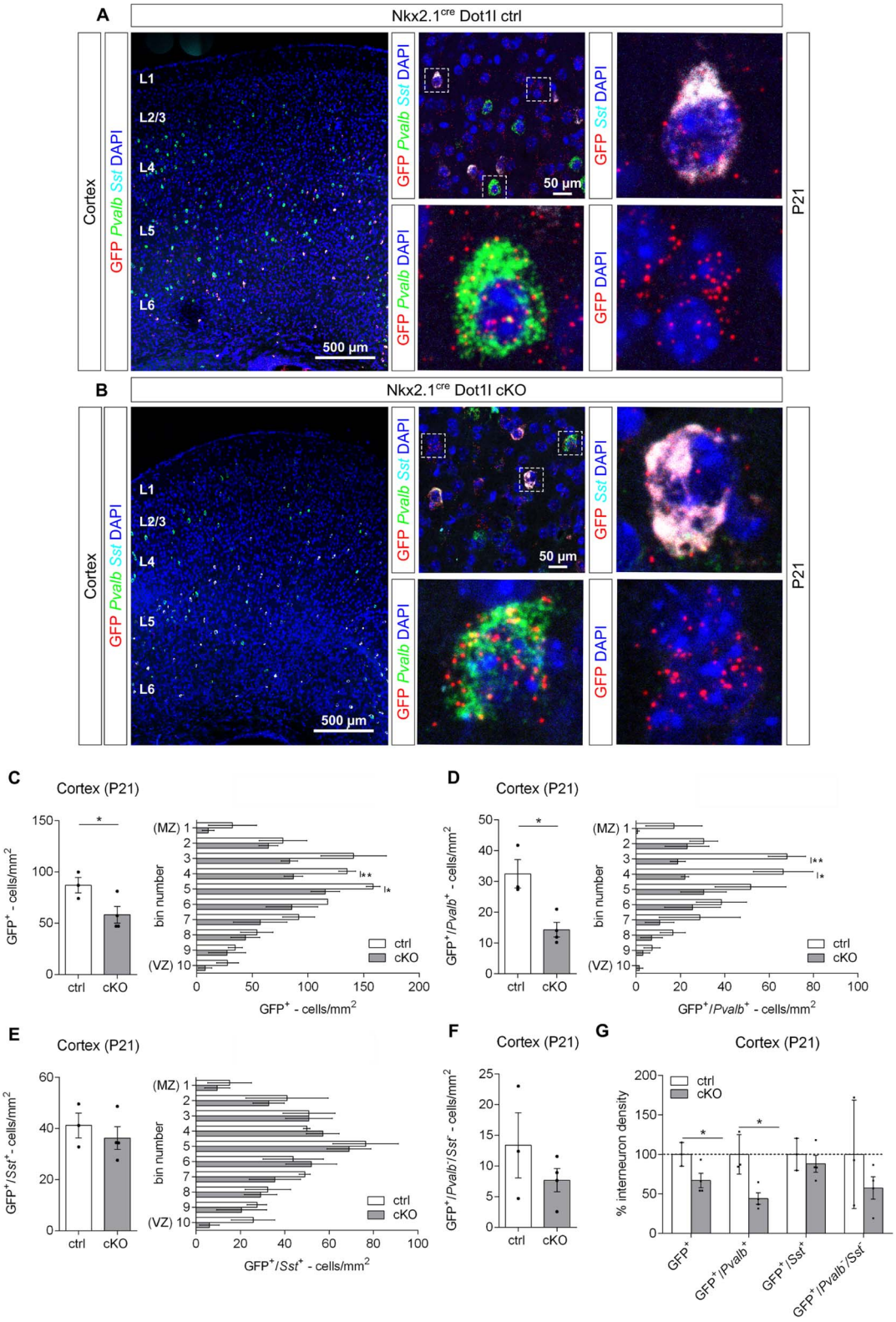

Fig. 5. *Dot1l* deletion in the Nkx2.1-cre lineage reduces the number of cortical *Pvalb*-expressing interneurons at P21. A, B) Representative images of *Pvalb*, *Sst*, and GFP expressing *Nkx2.1*-derived interneurons using smFISH at P21; $n = 3$–4 (Nkx2.1^{cre} Dot1l ctrl and cKO animals). Scale bar: 500 μm. Higher magnification of representative images of cerebral cortex regions, and higher magnifications of individual *Pvalb* (green), *Sst* (cyan) or GFP (red) expressing GABAergic interneurons together with DAPI (blue), and the combination of all (merge). Scale bar: 50 μm. C–E) Quantification of total *Nkx2.1*-derived interneurons (GFP$^+$ – cells), *Pvalb*- and *Sst*-expressing in the cortex and within each individual bin out of 10 bins spanning the entire cortex from VZ (bin 10) to the marginal zone (bin 1), of Nkx2.1^{cre} Dot1l cKO animals compared to controls at P21. Data are represented as the mean ± SEM; $n = 3$–4 (Nkx2.1^{cre} Dot1l ctrl and cKO animals); *$P < 0.05$ by unpaired, 2-tailed Student's *t*-test with Welch's correction. F) Quantification of interneurons expressing GFP alone in the cerebral cortex of Nkx2.1^{cre} Dot1l cKO animals compared to controls at P21. Data are represented as the mean ± SEM; $n = 3$–4 (Nkx2.1^{cre} Dot1l ctrl and cKO animals). G) Percentage of interneuron density in cKO mice compared to controls. Data are represented as the mean ± SEM; $n = 3$–4 (Nkx2.1^{cre} Dot1l ctrl and cKO animals); *$P < 0.05$ by unpaired, 2-tailed Student's *t*-test with Welch's correction.

(Supplementary Fig. S10A and B). We thus investigated whether the reduced proliferation of MGE progenitors at E14.5 would be involved in reducing the numbers of *Pvalb*-expressing interneurons. For that, pregnant mice at E14.5 received a 1-h BrdU pulse to label the cells in the S-phase of the cell cycle, and the numbers of BrdU- and Ki67-positive cells were determined. A significant decrease in the number of cycling progenitors ($BrdU^+$ $Ki67^+$ cells) was observed upon *Dot1l* cKO (1687.0 ± 320.8 cells/mm^2 vs. 4634.0 ± 927.6 cells/mm^2; $^*P < 0.05$), alongside an increased number of cells in the leaving fraction, as indicated by the increased ratio of $BrdU^+$ $Ki67^-$ cells/total $BrdU^+$ cells ($69.22 \pm 4.01\%$ vs. $52.14 \pm 5.43\%$; $^*P < 0.05$) (Fig. 6A and B). In addition, we observed a significant decrease in the numbers of mitotic PHH3-positive cells in the VZ of cKO mice (132.3 ± 27.25 cells/mm^2 vs. 225.4 ± 30.30 cells/mm^2; $^*P < 0.05$) (Fig. 6C and D). Since *Nkx2.1*-positive progenitors from the POA give rise to a smaller fraction of cortical interneurons (Gelman et al. 2009), we asked whether the reduced number of *Pvalb*-expressing interneurons might also be owing to reduced proliferation in the POA of cKO mice. However, neither the numbers of *Nkx2.1*-expressing progenitors nor PHH3-positive cells in the POA of cKO animals showed a statistically significant difference when compared to control mice (Supplementary Fig. S11). These experiments indicate that the decreased proliferation of MGE progenitors and premature cell cycle exit contribute to the decreased numbers of interneurons upon *Dot1l* deletion.

Taking all data together, we conclude that DOT1L keeps up the MGE progenitor pool to secure the generation of the latest interneurons from this region, i.e. MGE-derived PVALB expressing interneurons. DOT1L is involved in interneuron development by regulating cellular proliferation, maturation, and/or migration.

Discussion

In this work, we used two different cKO mouse models, namely Foxg1^{cre} Dot1l and Nkx2.1^{cre} Dot1l cKO lines, to establish that the epigenetic modifier DOT1L affects the embryonic and postnatal development of interneurons. *Dot1l* deletion in forebrain progenitors through Foxg1-cre affected the transcriptional programs in both MGE- and CGE-derived interneurons. *Dot1l* deletion in the MGE through Nkx2.1-cre resulted in reduced numbers of interneurons in cKO mice compared to control animals. Specifically, loss of *Dot1l* in *Nkx2.1*-expressing progenitors impaired the *Pvalb*-expressing subpopulation of interneurons, which reduced in numbers postnatally. Moreover, upon the loss of *Dot1l*, the reduced proliferation due to premature cell cycle exit was observed, which is in line with the fact that genes related to the cell cycle decreased, while the expression of neuronal markers increased. This finding strongly pointed toward cellular proliferation, neuronal differentiation, or specification/maturation defects as the possible underlying mechanisms.

That *Dot1l* deletion in *Foxg1*-expressing cells had broader effects on the interneuron development regarding the affected populations might reflect the fact that *Foxg1* has a wider expression in the ganglionic eminences, being expressed by both MGE- and CGE-derived cells (Dou et al. 1999). For the DEGs shared by our two models, we also observed that the transcriptional changes were usually stronger for the Foxg1^{cre} Dot1l cKO when compared to the Nkx2.1^{cre} Dot1l cKO mouse model. A reason for this difference might be that the bulk RNA sequencing data for Foxg1^{cre} Dot1l control and cKO mice were obtained from the dorsal telencephalon and that the *Dot1l* deletion in this model was not only restricted to GABAergic progenitors alone but also encompassed glutamatergic progenitors. The loss of DOT1L in both progenitor populations adds another source impacting interneuron development, namely the environment sensed by the cells and cell-to-cell interactions (Achim et al. 2014; Brandão and Romcy-Pereira 2015). The microenvironment might be differentially shaped in Foxg1^{cre}-mediated *Dot1l*, and the interneurons devoid of the epigenetic modifier entered a misspecified target region. It is thus tempting to speculate, but beyond the scope of this paper, that restricted deletion of *Dot1l* in the CP will impact interneuron development as well.

Dot1l deletion in MGE progenitor cells interfered specifically with the development of *Pvalb*-expressing interneurons. We cannot fully explain this observation based on our data as of yet. However, decreased proliferation seems to contribute to the reduction of *Pvalb*-expressing interneurons (Fig. 6), as indicated by the decreased proliferation, increased cell cycle exit, and the reduced number of mitotic cells at E14.5 (Fig. 6). We provided strong evidence in other parts of the CNS that DOT1L is crucial for maintaining the progenitor pool and consequently suitable neuronal numbers. For example, either pharmacological inhibition or short hairpin RNA-mediated knockdown of DOT1L results in the decreased proliferation of primary cortical neural stem cells (Roidl et al. 2016). Similar results were recapitulated by in vitro neuronal differentiation of NPCs derived from mouse embryonic stem cells upon the pharmacological inhibition of DOT1L, where DOT1L keeps the NPCs in a proliferative state through a mechanism dependent on the accessibility of SOX2-bound enhancers (Ferrari et al. 2020). Moreover, genetic deletion of *Dot1l* in the glutamatergic lineage led to an increased cell cycle exit (Franz et al. 2019). Since *Pvalb* interneurons are born later than the *Sst*-expressing subpopulations (Wonders et al. 2008; Inan et al. 2012), it is tempting to speculate that the reduced numbers of, specifically, *Pvalb* interneurons are caused by a slight reduction of the progenitor pool, which manifests in the last subpopulation generated, i.e. *Pvalb*-expressing interneurons.

In addition to temporal differences, spatial information could contribute to the *Pvalb*-specific effect of *Dot1l* deletion on the interneuron development. The dorsal part from the MGE produces mostly SST-positive interneurons, and progenitors from the ventral MGE give rise to PVALB-positive interneurons (Wonders et al. 2008). It is thus tempting to speculate that *Dot1l* deletion influences differently the cell fate decisions in the dorsal and ventral MGE, with the ventral MGE being more affected than the dorsal MGE. However, we did not observe changes in the expression of the dorsal MGE marker *Nkx6.2* (Supplementary Fig. S6C). Moreover, there is no significant difference between the *Sst*-expressing fractions of control and cKO mice at P21, ruling out a fate switch identity from PVALB to SST as the reason to observe a decreased number of *Pvalb*-positive interneurons upon *Dot1l* cKO (Fig. 5G). This is in agreement with our analysis on the expression of earlier markers for PVALV interneurons at embryonic stages where no differences were observed between genotypes (Supplementary Fig. S9). In addition, a fate switch from a cortical to a striatal identity due to the reduced expression of *Nkx2.1* upon *Dot1l* cKO does not seem to be the involved mechanism. If so, we would expect to observe an increased number of cortical interneurons, and therefore, fewer striatal interneurons since *Nkx2.1* is downregulated in interneurons destined to the cortex, while its expression persists in interneurons migrating to the striatum (Nóbrega-Pereira et al. 2008). However, we observed a decrease in both cortical and striatal interneurons at P0 (Fig. 4). One could also argue that the reduced number of *Pvalb*-positive interneurons only reflects a delay in the maturation of these neurons, and consequently, a reduced expression of *Pvalb* expression at P21.

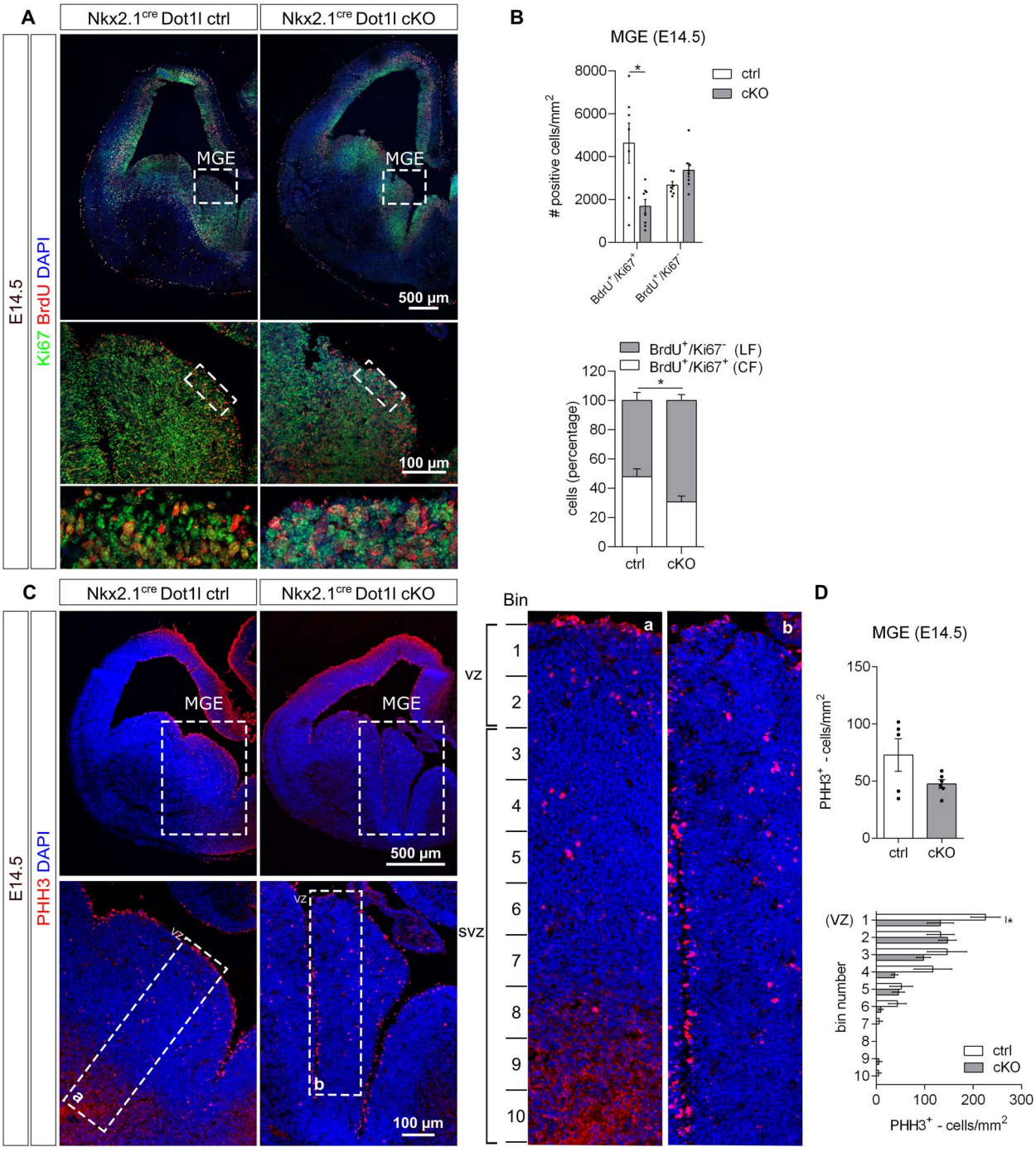

Fig. 6. *Dot1l* deletion in the Nkx2.1-cre lineage induces premature cell cycle exit and reduces the number of mitotic cells at embryonic E14.5. A) Representative images of immunostaining of E14.5 forebrain sections for BrdU (red), Ki67 (green), and DAPI (blue). Scale bars: 500 μm (upper panel) and 100 μm (magnification). BrdU injections were performed 1 h prior brain dissection. B) Cell density of BrdU$^+$/Ki67$^+$ and BrdU$^+$/Ki67$^-$cells in the MGE of Nkx2.1^{cre} Dot1l control ($n = 7$) and cKO ($n = 8$) animals at E14.5 (upper panel). Lower panel: determination of the cell cycle exit index (BrdU$^+$ Ki67$^-$ cells/total BrdU$^+$ cells ratio—leaving fraction—LF) and the cycling fraction (CF, BrdU$^+$ Ki67$^+$ cells/total BrdU$^+$ cells ratio). C) Representative images of PHH3-positive MGE-derived cells at E14.5; $n = 5$–6 (Nkx2.1^{cre} Dot1l ctrl and cKO animals). Scale bar: 500 μm. Higher magnifications of representative images, depicting the MGE and counted area. Scale bar: 100 μm. Higher magnifications of the areas used for quantification. Scale bar: 50 μm. D) Quantification of total PHH3-positive MGE-derived cells and within each individual bin out of 10 bins, starting from bin 1 (VZ), of Nkx2.1^{cre} Dot1l cKO animals compared to controls at E14.5. Data are represented as the mean ± SEM; $n = 5$–6 (Nkx2.1^{cre} Dot1l ctrl and cKO animals); *$P < 0.05$ by unpaired, 2-tailed Student's *t*-test with Welch's correction.

If this was the case, we would expect to observe an increased fraction of cells expressing GFP alone. However, the control and cKO mice are indistinguishable regarding that (Fig. 5F and G).

By using BrdU birthdating experiments combined with transplantation studies, different authors have shown that, while SST-expressing interneurons are mostly generated at earlier time points (E12.5/13.5), PVALB-expressing interneurons are continuously born between E12.5 and E15.5 (Wonders et al. 2008; Inan et al. 2012). This is in agreement with the observation that the fate specification of interneurons is also related to the

location of neurogenesis in the MGE. SST-expressing interneurons are mostly generated from apical progenitors in the ventricular zone, whereas late CCND2-expressing basal progenitors in the subventricular zone mostly give rise to PVALB-expressing interneurons (Petros et al. 2015). *Ccnd2* was one target gene with decreased expression upon *Dot1l* deletion in the MGE (Fig. 3D). We therefore hypothesize that *Dot1l* cKO-induced reduction in the number of *Pvalb*-expressing interneurons is due to a reduction of the basal progenitor pool, which results from the reduced proliferation of apical progenitors and their premature cell cycle exit followed by differentiation into *Sst*-expressing interneurons before the transition to basal progenitors. This scenario would explain the discrete tendency to decreased numbers of *Sst*-expressing interneurons, while the statistical significance for *Pvalb*-expressing interneurons was reached. In favor of this interpretation is our earlier report that, upon *Dot1l* cKO, cortical progenitor cells exit the cell cycle prematurely and adapt the DL neuron fate. At the time of the transition from apical to basal progenitors, there are less apical and consequently less TBR2-positive basal progenitors to give rise to UL neurons (Franz et al. 2019). Supporting our hypothesis is also the recent observation that the cortical interneuron populations result from a postmitotic lineage divergence. Interneurons derive from a common progenitor pool with limited heterogeneity, and, soon after cell cycle exit, different transcriptional programs refine the trajectories taken by the postmitotic interneurons and, consequently, their identities (Bandler et al. 2022).

Additionally, we observed an aberrant lamination of cortical glutamatergic DL neurons (Franz et al. 2019), which might also parallel some of our observations regarding the mislocalization of MGE-derived interneurons upon *Dot1l* cKO that mainly populated superficial layers of the CP, i.e. layers 4–6, at least at P0 (Fig. 4E and F). PVALB-positive neurons settle preferentially between layers 1 and 2 (Miyamae et al. 2017), and we observed fewer neurons in these layers upon the loss of DOT1L. The mislocalization of interneurons might thus reflect an accelerated or premature neuronal differentiation, and subsequently, earlier invasion of the interneurons in the CP concomitant with a failure to adapt a mature PVALB fate. Moreover, PVALB-positive interneurons derived from the MGE at earlier stages (E12.5) tend to occupy deep cortical layers, while those ones generated at later stages (E14.5) settle in more superficial layers (Ciceri et al. 2013). This reinforces the notion that the generation of the latest PVALB interneurons might be impaired upon *Dot1l* deletion, which is in line with our observation of fewer PVALB-expressing interneurons in superficial cortical layers in contrast to similar numbers of interneurons settling in DLs (Fig. 5D). Taking into account the observed decreased expression of genes related to cell cycle, including the basal progenitor marker and the increased activity of genes involved in late neuronal maturation (Fig. 3, Supplementary Fig. S4), the maintenance of the progenitor pool by DOT1L might also play an important role in the development of MGE-derived interneurons, as we observed for cortical glutamatergic neurons.

The altered distribution of MGE-derived interneurons in the CP at P0 upon *Dot1l* deletion (Fig. 4E and F) might not only indicate premature differentiation and invasion of the CP but also impaired postmitotic maturation. One possible mechanism might be attributed to the decreased expression of *Ackr3* in the vT from Nkx2.1^{cre}Dotl1 cKO mice at E14.5 (Fig. 3D, Supplementary Fig. S4I). ACKR3 (also known as CXCR7) is a CXCL12 receptor expressed by migrating interneurons, and this chemokine signaling pathway is important for proper interneuron migration (López-Bendito et al. 2008; Sánchez-Alcañiz et al. 2011; Bartolini et al. 2017). Interneurons of *Ackr3*$^{-/-}$ mice leave the MZ and the SVZ to accumulate in the CP. Thus, one might speculate that the reduced expression of *Ackr3* upon *Dot1l* deletion in MGE-derived interneurons is involved in their aberrant laminar distribution in the CP.

Conclusion

Summing up, our results indicate that reduced numbers of cortical interneurons upon *Dot1l* deletion might result from premature differentiation alongside reduction of the progenitor pool due to earlier cell cycle exit. The depletion of progenitors mainly affected the later interneuron populations that express *Pvalb* and settle in more superficial layers of the developing CP compared to earlier stages. Additional research to address open, mechanistic questions will be needed to increase our understanding on the epigenetics and DOT1L functions governing the GABAergic development in normal and disease conditions.

Acknowledgments

We thank C. Fullio for her help plotting data with "R" and S. Heinrich for her help with animal work. Further, the authors thank the Freiburg Galaxy Server team and all members of the Vogel group for discussion and support.

Supplementary material

Supplementary material is available at *Cercor* online.

CRediT author statement

Arquimedes Cheffer (Data curation, Formal analysis, Investigation, Writing—original draft, Writing—review & editing), Marta Garcia-Miralles (Data curation, Formal analysis, Investigation, Writing—original draft, Writing—review & editing), Esther Maier (Data curation, Formal analysis, Investigation, Writing—review & editing), Ipek Akol (Data curation, Formal analysis, Writing—review & editing), Henriette Franz (Investigation), Vandana Shree Vedartham Srinivasan (Investigation, Writing—review & editing), and Tanja Vogel (Conceptualization, Data curation, Formal analysis, Funding acquisition, Methodology, Project administration, Resources, Supervision, Validation, Writing—review & editing)

Funding

This work was supported by the Deutsche Forschungsgemeinschaft (DFG) through a grant to TV (VO1676/7-1).

Conflict of interest statement: None declared.

Data availability

The raw sequencing files were deposited to the NCBI Gene Expression Omnibus (GEO) with accession number GSE221994. All other data types and codes recreating the analyses from the data files can be found at https://github.com/Vogel-lab/DOT1L-interneuron-development as R markdown files and at Galaxy workflows.

References

Achim K, Salminen M, Partanen J. Mechanisms regulating GABAergic neuron development. *Cell Mol Life Sci*. 2014:71(8):1395–1415.

Afgan E, Nekrutenko A, Grüning BA, Blankenberg D, Goecks J, Schatz MC, Ostrovsky AE, Mahmoud A, Lonie AJ, Syme A, et al. The galaxy platform for accessible, reproducible and collaborative biomedical analyses: 2022 update. *Nucleic Acids Res*. 2022:50(W1): W345–W351.

Asgarian Z, Magno L, Ktena N, Harris KD, Kessaris N. Hippocampal CA1 somatostatin interneurons originate in the embryonic MGE/POA. *Stem cell reports*. 2019:13(5):793–802.

Asgarian Z, Oliveira MG, Stryjewska A, Maragkos I, Rubin AN, Magno L, Pachnis V, Ghorbani M, Hiebert SW, Denaxa M, et al. MTG8 interacts with LHX6 to specify cortical interneuron subtype identity. *Nat Commun*. 2022:13(1):5217.

Bandler RC, Vitali I, Delgado RN, Ho MC, Dvoretskova E, Ibarra Molinas JS, Frazel PW, Mohammadkhani M, Machold R, Maedler S, et al. Single-cell delineation of lineage and genetic identity in the mouse brain. *Nature*. 2022:601(7893):404–409.

Bartolini G, Sánchez-Alcañiz JA, Osório C, Valiente M, García-Frigola C, Marín O. Neuregulin 3 mediates cortical plate invasion and laminar allocation of GABAergic interneurons. *Cell Rep*. 2017:18(5):1157–1170.

Blighe K, Rana S LM. EnhancedVolcano: publication-ready volcano plots with enhanced colouring and labeling. 2022. R package version 1.16.0. https://github.com/kevinblighe/EnhancedVolcano.

Bovio PP, Franz H, Heidrich S, Rauleac T, Kilpert F, Manke T, Vogel T. Differential methylation of H3K79 reveals DOT1L target genes and function in the cerebellum in vivo. *Mol Neurobiol*. 2019:56(6): 4273–4287.

Brandão JA, Romcy-Pereira RN. Interplay of environmental signals and progenitor diversity on fate specification of cortical GABAergic neurons. *Front Cell Neurosci*. 2015:9:149.

Büttner N, Johnsen SA, Kügler S, Vogel T. Af9/Mllt3 interferes with Tbr1 expression through epigenetic modification of histone H3K79 during development of the cerebral cortex. *Proc Natl Acad Sci U S A*. 2010:107(15):7042–7047.

Chen Y-JJ, Friedman BA, Ha C, Durinck S, Liu J, Rubenstein JL, Seshagiri S, Modrusan Z. Single-cell RNA sequencing identifies distinct mouse medial ganglionic eminence cell types. *Sci Rep*. 2017:7:45656.

Ciceri G, Dehorter N, Sols I, Huang ZJ, Maravall M, Marín O. Lineage-specific laminar organization of cortical GABAergic interneurons. *Nat Neurosci*. 2013:16(9):1199–1210.

Dou CL, Li S, Lai E. Dual role of brain factor-1 in regulating growth and patterning of the cerebral hemispheres. *Cereb Cortex*. 1999:9(6): 543–550.

Faux C, Rakic S, Andrews W, Britto JM. Neurons on the move: migration and lamination of cortical interneurons. *Neurosignals*. 2012:20(3):168–189.

Ferrari F, Arrigoni L, Franz H, Izzo A, Butenko L, Trompouki E, Vogel T, Manke T. DOT1L-mediated murine neuronal differentiation associates with H3K79me2 accumulation and preserves SOX2-enhancer accessibility. *Nat Commun*. 2020:11(1):5200.

Flames N, Pla R, Gelman DM, Rubenstein JLR, Puelles L, Marín O. Delineation of multiple subpallial progenitor domains by the combinatorial expression of transcriptional codes. *J Neurosci*. 2007:27(36):9682–9695.

Franz H, Villarreal A, Heidrich S, Videm P, Kilpert F, Mestres I, Calegari F, Backofen R, Manke T, Vogel T. DOT1L promotes progenitor proliferation and primes neuronal layer identity in the developing cerebral cortex. *Nucleic Acids Res*. 2019:47(1):168–183.

Gelman DM, Martini FJ, Nóbrega-Pereira S, Pierani A, Kessaris N, Marín O. The embryonic preoptic area is a novel source of cortical GABAergic interneurons. *J Neurosci*. 2009:29(29):9380–9389.

Gray de Cristoforis A, Ferrari F, Clotman F, Vogel T. Differentiation and localization of interneurons in the developing spinal cord depends on DOT1L expression. *Mol Brain*. 2020:13(1):85.

Hébert JM, McConnell SK. Targeting of cre to the Foxg1 (BF-1) locus mediates loxP recombination in the telencephalon and other developing head structures. *Dev Biol*. 2000:222(2):296–306.

Inan M, Welagen J, Anderson SA. Spatial and temporal bias in the mitotic origins of somatostatin- and parvalbumin-expressing interneuron subgroups and the chandelier subtype in the medial ganglionic eminence. *Cereb Cortex*. 2012:22(4):820–827.

Juliandi B, Abematsu M, Nakashima K. Epigenetic regulation in neural stem cell differentiation. *Develop Growth Differ*. 2010:52(6): 493–504.

Kawakami Y, Esteban CR, Matsui T, Rodríguez-León J, Kato S, Belmonte JCI. Sp8 and Sp9 , two closely related buttonhead -like transcription factors, regulate Fgf8 expression and limb outgrowth in vertebrate embryos. *Development*. 2004:131(19): 4763–4774.

Kolde R. Pheatmap: pretty heatmaps. 2019. R package version 1.0. 12. https://rdrr.io/cran/pheatmap/.

Kronman H, Torres-Berrío A, Sidoli S, Issler O, Godino A, Ramakrishnan A, Mews P, Lardner CK, Parise EM, Walker DM, et al. Long-term behavioral and cell-type-specific molecular effects of early life stress are mediated by H3K79me2 dynamics in medium spiny neurons. *Nat Neurosci*. 2021:24(5):667–676.

Lavdas AA, Grigoriou M, Pachnis V, Parnavelas JG. The medial ganglionic eminence gives rise to a population of early neurons in the developing cerebral cortex. *J Neurosci*. 1999:19(18):7881–7888.

Lim L, Mi D, Llorca A, Marín O. Development and functional diversification of cortical interneurons. *Neuron*. 2018:100(2):294–313.

Limoni G, Murthy S, Jabaudon D, Dayer A, Niquille M. PlexinA4-Semaphorin3A-mediated crosstalk between main cortical interneuron classes is required for superficial interneuron lamination. *Cell Rep*. 2021:34(4):108644.

Liodis P, Denaxa M, Grigoriou M, Akufo-Addo C, Yanagawa Y, Pachnis V. Lhx6 activity is required for the normal migration and specification of cortical interneuron subtypes. *J Neurosci*. 2007:27(12): 3078–3089.

López-Bendito G, Sánchez-Alcañiz JA, Pla R, Borrell V, Picó E, Valdeolmillos M, Marín O. Chemokine signaling controls intracortical migration and final distribution of GABAergic interneurons. *J Neurosci*. 2008:28(7):1613–1624.

Love MI, Huber W, Anders S. Moderated estimation of fold change and dispersion for RNA-seq data with DESeq2. *Genome Biol*. 2014:15(12):550.

Marín O, Rubenstein JL. A long, remarkable journey: tangential migration in the telencephalon. *Nat Rev Neurosci*. 2001:2(11): 780–790.

Mayer C, Hafemeister C, Bandler RC, Machold R, Batista Brito R, Jaglin X, Allaway K, Butler A, Fishell G, Satija R. Developmental diversification of cortical inhibitory interneurons. *Nature*. 2018:555(7697):457–462.

Meyer HS, Schwarz D, Wimmer VC, Schmitt AC, Kerr JND, Sakmann B, Helmstaedter M. Inhibitory interneurons in a cortical column form hot zones of inhibition in layers 2 and 5A. *Proc Natl Acad Sci U S A*. 2011:108(40):16807–16812.

Mi D, Li Z, Lim L, Li M, Moissidis M, Yang Y, Gao T, Hu TX, Pratt T, Price DJ, et al. Early emergence of cortical interneuron diversity in the mouse embryo. *Science*. 2018:360(6384):81–85.

Miyamae T, Chen K, Lewis DA, Gonzalez-Burgos G. Distinct physiological maturation of parvalbumin-positive neuron subtypes in mouse prefrontal cortex. *J Neurosci*. 2017:37(19):4883–4902.

Miyoshi G, Fishell G. GABAergic interneuron lineages selectively sort into specific cortical layers during early postnatal development. *Cereb Cortex*. 2011:21(4):845–852.

Miyoshi G, Ueta Y, Natsubori A, Hiraga K, Osaki H, Yagasaki Y, Kishi Y, Yanagawa Y, Fishell G, Machold RP, et al. FoxG1 regulates the formation of cortical GABAergic circuit during an early postnatal critical period resulting in autism spectrum disorder-like phenotypes. *Nat Commun*. 2021:12(1):3773.

Mo A, Mukamel EA, Davis FP, Luo C, Henry GL, Picard S, Urich MA, Nery JR, Sejnowski TJ, Lister R, et al. Epigenomic signatures of neuronal diversity in the mammalian brain. *Neuron*. 2015:86(6): 1369–1384.

MuhChyi C, Juliandi B, Matsuda T, Nakashima K. Epigenetic regulation of neural stem cell fate during corticogenesis. *Int J Dev Neurosci*. 2013:31(6):424–433.

Nahar L, Delacroix BM, Nam HW. The role of parvalbumin interneurons in neurotransmitter balance and neurological disease. *Front Psychiatry*. 2021:12:679960.

Nóbrega-Pereira S, Kessaris N, Du T, Kimura S, Anderson SA, Marín O. Postmitotic Nkx2-1 controls the migration of telencephalic interneurons by direct repression of guidance receptors. *Neuron*. 2008:59(5):733–745.

Petros TJ, Bultje RS, Ross ME, Fishell G, Anderson SA. Apical versus basal neurogenesis directs cortical interneuron subclass fate. *Cell Rep*. 2015:13(6):1090–1095.

Prévot T, Sibille E. Altered GABA-mediated information processing and cognitive dysfunctions in depression and other brain disorders. *Mol Psychiatry*. 2021:26(1):151–167.

Rakic P. Radial versus tangential migration of neuronal clones in the developing cerebral cortex. *Proc Natl Acad Sci U S A*. 1995:92(25): 11323–11327.

Roidl D, Hellbach N, Bovio PP, Villarreal A, Heidrich S, Nestel S, Grüning BA, Boenisch U, Vogel T. DOT1L activity promotes proliferation and protects cortical neural stem cells from activation of ATF4-DDIT3-mediated ER stress in vitro. *Stem Cells*. 2016:34(1): 233–245.

Ruden JB, Dugan LL, Konradi C. Parvalbumin interneuron vulnerability and brain disorders. *Neuropsychopharmacology*. 2021:46(2): 279–287.

Sánchez-Alcañiz JA, Haege S, Mueller W, Pla R, Mackay F, Schulz S, López-Bendito G, Stumm R, Marín O. Cxcr7 controls neuronal migration by regulating chemokine responsiveness. *Neuron*. 2011:69(1):77–90.

Sandberg M, Flandin P, Silberberg S, Su-Feher L, Price JD, Hu JS, Kim C, Visel A, Nord AS, Rubenstein JLR. Transcriptional networks controlled by NKX2-1 in the development of forebrain GABAergic neurons. *Neuron*. 2016:91(6):1260–1275.

Shen L, Nam H-S, Song P, Moore H, Anderson SA. FoxG1 haploinsufficiency results in impaired neurogenesis in the postnatal hippocampus and contextual memory deficits. *Hippocampus*. 2006:16(10):875–890.

Siddiqi F, Trakimas AL, Joseph DJ, Lippincott ML, Marsh ED, Wolfe JH. Islet1 precursors contribute to mature interneuron subtypes in mouse neocortex. *Cereb Cortex*. 2021:31(11):5206–5224.

Srinivas S, Watanabe T, Lin CS, William CM, Tanabe Y, Jessell TM, Costantini F. Cre reporter strains produced by targeted insertion of EYFP and ECFP into the ROSA26 locus. *BMC Dev Biol*. 2001:1:4.

Tremblay R, Lee S, Rudy B. GABAergic interneurons in the neocortex: from cellular properties to circuits. *Neuron*. 2016:91(2): 260–292.

Wester JC, Mahadevan V, Rhodes CT, Calvigioni D, Venkatesh S, Maric D, Hunt S, Yuan X, Zhang Y, Petros TJ, et al. Neocortical projection neurons instruct inhibitory interneuron circuit development in a lineage-dependent manner. *Neuron*. 2019:102(5): 960–975.e6.

Wonders CP, Anderson SA. The origin and specification of cortical interneurons. *Nat Rev Neurosci*. 2006:7(9):687–696.

Wonders CP, Taylor L, Welagen J, Mbata IC, Xiang JZ, Anderson SA. A spatial bias for the origins of interneuron subgroups within the medial ganglionic eminence. *Dev Biol*. 2008:314(1):127–136.

Wu T, Hu E, Xu S, Chen M, Guo P, Dai Z, Feng T, Zhou L, Tang W, Zhan L, et al. clusterProfiler 4.0: a universal enrichment tool for interpreting omics data. *Innovation (Camb)*. 2021:2(3):100141.

Xu Q, Tam M, Anderson SA. Fate mapping Nkx2.1-lineage cells in the mouse telencephalon. *J Comp Neurol*. 2008:506(1):16–29.